Heterobivalent ligands target cell-surface receptor combinations in vivo

Liping Xu[a], Jatinder S. Josan[b,c], Josef Vagner[c], Michael R. Caplan[d], Victor J. Hruby[b,c], Eugene A. Mash[b], Ronald M. Lynch[e], David L. Morse[a], and Robert J. Gillies[a,1]

[a]Department of Cancer Imaging and Metabolism, H. Lee Moffitt Cancer Center and Research Institute, Tampa, FL 33612; [b]Department of Chemistry and Biochemistry, University of Arizona, Tucson, AZ 85721; [c]Bio 5 Institute, University of Arizona, Tucson, AZ 85719; [d]Harrington Department of Bioengineering, Arizona State University, Tempe, AZ 85287-9709; and [e]Department of Physiology, University of Arizona, Tucson, AZ 85724

Edited* by Donald M. Engelman, Yale University, New Haven, CT, and approved October 18, 2012 (received for review July 19, 2012)

A challenge in tumor targeting is to deliver payloads to cancers while sparing normal tissues. A limited number of antibodies appear to meet this challenge as therapeutics themselves or as drug-antibody conjugates. However, antibodies suffer from their large size, which can lead to unfavorable pharmacokinetics for some therapeutic payloads, and that they are targeted against only a single epitope, which can reduce their selectivity and specificity. Here, we propose an alternative targeting approach based on patterns of cell surface proteins to rationally develop small, synthetic heteromultivalent ligands (htMVLs) that target multiple receptors simultaneously. To gain insight into the multivalent ligand strategy in vivo, we have generated synthetic htMVLs that contain melanocortin (MSH) and cholecystokinin (CCK) pharmacophores that are connected via a fluorescent labeled, rationally designed synthetic linker. These ligands were tested in an experimental animal model containing tumors that expressed only one (control) or both (target) MSH and CCK receptors. After systemic injection of the htMVL in tumor-bearing mice, label was highly retained in tumors that expressed both, compared with one, target receptors. Selectivity was quantified by using ex vivo measurement of Europium-labeled htMVL, which had up to 12-fold higher specificity for dual compared with single receptor expressing cells. This proof-of-principle study provides in vivo evidence that small, rationally designed bivalent htMVLs can be used to selectively target cells that express both, compared with single complimentary cell surface targets. These data open the possibility that specific combinations of targets on tumors can be identified and selectively targeted using htMVLs.

receptor targeting | multivalency | cross-linking | gene expression profiling

Since it was first described by Paul Erhlich, the search for a "magic bullet" drug that kills cancer cells while leaving normal cells unaffected has inspired generations of scientists. As targeted deliveries of therapies become more developed, some have shown clinical, albeit short-lived, success (1, 2). The majority of targeted anticancer approaches rely on high-affinity monovalent interactions between a cell-targeted agent (monoclonal or recombinant antibodies and peptides) and a tumor-associated protein to direct therapeutic or imaging payload selectively to the tumors (3–5). In contrast, multivalent interactions have been shown to exhibit higher binding avidities, compared with the monovalent interactions (6–8). Thus, homomultivalent drugs (i.e., multiple copies of the same pharmacophores) have become increasingly common for targeted therapeutic and imaging agents with improved avidity and higher specificity (9, 10). We have proposed (11) and have shown in vitro (12) that heterobivalent ligands designed to noncovalently cross-link two different membrane receptors can provide greater selectivity than homobivalent ligands while retaining the high avidity of multimeric interactions. This observation has also been shown by others with a single bispecific antibodies targeting, e.g., epidermal growth factor (HER2) and vascular endothelial growth factor receptors (13, 14). Although antibody-based drugs are the fastest-growing class of protein therapeutics in clinical development, they are limited by their large size, leading to poor tissue penetrance and long serum retention times. This limitation has inspired attempts to create smaller binding proteins with high avidity, based on nonantibody scaffolded targeting agents.

Here, we present an alternative multivalent targeting approach based on cell surface expressed protein patterns, developing rationally designed synthetic heteromultivalent ligands (htMVLs) wherein high selectivity can be achieved through multivalency for target cells (11, 15, 16). Such an approach is a unique application of pharmacogenomics, in which cell surface protein markers that are simultaneously present on the surface at threshold concentrations can be targeted in combination. From set theory (Fig. S1*A*), the number of targetable receptor combinations is $\sim 2{,}500^n$, where 2,500 is the approximate number of targetable cell surface receptors and n is the valency of the targeting ligand (17). Nontarget tissues can thus be discriminated by the lack of such receptor combinations. Furthermore, such an approach does not require the targets to be highly overexpressed by the target cells to ensure specificity (15). We have characterized and validated numerous two-, three-, and four-receptor combinations in both pancreatic cancers and melanoma with expression profiling and immunohistochemistry (18).

To demonstrate the feasibility of a multivalent targeting approach, tumor cells have been engineered to express one or both of two different G protein-coupled receptors (GPCRs): the human melanocortin-1 receptor (MC1R) and the human cholecystokinin-2 receptor (CCK2R). Those cells expressing both are target cells, and those with only one receptor (either MC1R or CCK2R) are controls. If our hypothesis is correct, we expect that a heterobivalent ligand will bind with higher avidity to cells bearing both receptors compared with cells with only one (Fig. S1*A*).

We also designed and synthesized a series of htMVLs containing both MSH and CCK ligands. Previous in vitro studies demonstrated that these ligands bound to the target cells with higher affinity compared with control cells (17, 19), suggesting the ability to noncovalently cross-link heterologous receptors by using the htMVLs. The current study follows up on this prior in vitro work, by establishing an animal model for examining the tumor uptake and biodistribution of htMVLs. After systemic injection of Cy5 or Europium (Eu) chelated ligands, label was highly retained in tumors that expressed both, compared with one, target receptors. Selectivity was visualized and quantified to show that the small synthetic htMVLs can distinguish target cells from control cells. These data provide evidence that heterobivalent agents can be developed for in vivo targeting of human cancers.

Author contributions: L.X., J.S.J., V.J.H., R.M.L., D.L.M., and R.J.G. designed research; L.X., J.S.J., M.R.C., and R.M.L. performed research; J.V., V.J.H., E.A.M., and R.M.L. contributed new reagents/analytic tools; L.X., J.S.J., and M.R.C. analyzed data; and L.X., J.S.J., M.R.C., D.L.M., and R.J.G. wrote the paper.

The authors declare no conflict of interest.

*This Direct Submission article had a prearranged editor.

[1]To whom correspondence should be addressed. E-mail: robert.gillies@moffitt.org.

This article contains supporting information online at www.pnas.org/lookup/suppl/doi:10.1073/pnas.1211762109/-/DCSupplemental.

Results

Design, Synthesis, and Biological Activities of htMVLs. For the ligand design, a truncated version of NDP-α-MSH, i.e., Ser-Nle-Glu-His-DPhe-Arg-Trp (MSH7), was attached at the N terminus of a linker and, at the C terminus, was attached a modified version of CCK4 with both methionine residues replaced with norleucine, i.e., Nle-Gly-Trp-Nle-Asp-Phe (CCK6). Linker design was based on the crystal structure of GPCRs (20, 21). Three families of htMVLs were designed composed of semirigid Pro-Gly linkers and flexible PEGO linkers with the length ranging from 13 to 96 Å (17). From in vitro binding data (19), a core of three (Pro-Gly) repeats flanked by PEGO units (PEGO-$[PG]_3$-PEGO) showed maximal affinity with minimal size (58 atoms, modeled at 46 Å). In the current study, the fluorescent tags, including Cy5 (htMVL 1) and Eu (htMVL 2) (Fig. 1*A*) were incorporated with an intervening Lys in the center of the linker region. Ligands were purified by HPLC and characterized by MS (Table S1). Notably, linker components are biocompatible, inert, and have desirable solubility, pharmacokinetic, pharmacodynamic, and immunogenic properties (22–24). Molecular dynamic simulations of these ligands revealed significant conformational mobility of the linker unit and desired spacing range for pharmacophore binding under various receptor binding pocket orientations and spatial contexts as would be encountered on the cell surface (Fig. 1 *B–D*) (17).

To ensure the binding avidities of these ligands were not affected by the incorporation of the imaging tags, htMVL1 and htMVL2 were assayed for binding activity by using the stable Hek293 cells expressing either or both MC4R and CCK2R receptors (19). htMVL1 was assayed for competitive binding and htMVL2 assayed for saturation binding. These in vitro binding results showed that both ligands displayed bivalent/monovalent enhancement ratios of ~20-fold and ~twofold for MC4Rs and CCK2Rs, respectively (Table 1). Given the similar enhancement ratios, both of these compounds were brought forth for subsequent in vivo studies.

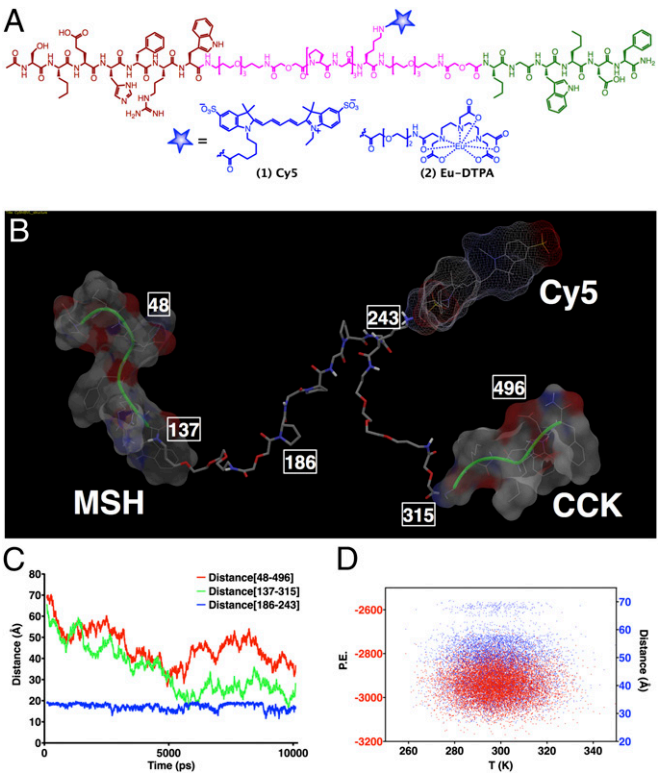

Fig. 1. Chemical structures of labeled compounds and their molecular dynamic profiling for assessing ligand mobility. (*A*) Heterobivalent ligands containing melanocortin (brown) and cholecystokinin (green) pharmacophores connected via a PEGO-$[PG]_3$-PEGO linker (cyan) that bears a lysine handle for incorporation of Cy5 and Eu-DTPA tags (blue). (*B–D*) Molecular dynamic study of Cy5 labeled ligand 1 (htMVL 1). (*B*) Illustration of one of the conformers with various functionalities and atom labels that were monitored for distances during the simulation is shown in *C*, and energy plot of various conformations (distance mapped from atoms 48–496) against temperature is shown in *D*. The study reveals significant linker mobility with 30–70 Å spacing between the two motifs and an average distance range of 40 Å (see *SI Materials and Methods* for more details).

Construction and Characterization of Engineered Stable Tumor Cell Lines. For in vivo experiments, we engineered HCT116 cells to express both MC1R and CCK2R (HCT116/MC1R/CCK2R) as target cells, or only MC1R (HCT116/MC1R) or CCK2R (HCT116/CCK2R) as controls. All engineered cell lines were fully characterized for corresponding receptor expression (Fig. S2). Whole proteins from these cell lines were harvested and analyzed by Western blotting, which have shown the corresponding protein bands (Fig. S3*A*). Cell surface expression of these receptors was validated by immunocytochemistry (Fig. S3*B*). Receptor densities on the cell surface were determined by saturation binding using monovalent ligands, Eu-NDP-α-MSH and Eu-CCK-8 (Fig. S1*B*) for MC1R and CCK2R, respectively (19). These binding data (Fig. S2) showed that dual receptor cells had 180,000 ± 20,000 CCK2R and 10,000 ± 2,000 MC1R binding sites per cell, whereas HCT116/MC1R and HCT116/CCK2R cells contained 240,000 ± 60,000 and 190,000 ± 40,000 receptor binding sites per cell, respectively. To assess the penetrance of both receptors in the target cell population, flow cytometric analyses were performed with htMVL1, which showed that 90.6 ± 2.6% (n = 3) of the cells in the population were Cy5 positive (Fig. S3*C*).

Cy5 htMVL 1 Specifically Binds to Target Cells. To visualize the binding of htMVL 1 in vitro, we treated target and control cells with the ligand at different concentrations (Fig. 2*A*). Microscopically, there was a quantitative difference in the cellular uptake of the ligand between target and control cells. At 100 nM, 10 nM, and 1 nM, respectively, 80%, 50%, and 13% of the target cells bound appreciable ligand, whereas only 41%, 33%, and 0% of the MC1R control cells, and 69%, 35%, and 5% of the CCK2R control cells bound to the ligand (Fig. 2*B*). At the high dose treatment (100 nM), the difference between binding to the target cells and CCK2R control cells was not significantly different, probably owing to the high CCKR receptor number in both cells (Fig. 2*B*). To rule out nonspecific binding, blocking experiments (Fig. 2*C*) showed that NDP-α-MSH (Fig. S1*B*, ligand 3), CCK8 (Fig. S1*B*, ligand 4), or both significantly reduced the Cy5 signal by 17.4%, 92.0%, and 100%, respectively, compared with nonblocked target cells (Fig. 2 *C* and *D*). These results indicate that, at low concentrations, htMVL 1 was able to effectively discriminate dual-receptor and monoreceptor expressing cell lines in vitro, which was consistent with earlier observations (17, 19).

Furthermore, htMVL 1 appeared to be internalized, consistent with prior observations (25). For therapeutic and imaging payloads, ligand-mediated endocytosis is beneficial in that it can lead to signal amplification and deliver therapies directly into the target cells. However, it is possible that a rapidly internalizing single receptor cell line could thus achieve similar activities and, hence, reduce specificity. For this reason, doses of htMVLs must be kept very low to maximize the multivalent enhancement. A dynamic imaging series over 30 mins showed that the Cy5-labeled ligands bound to and were internalized into the target cell (Fig. 2*E*). At 1–2 min after treatment, the ligands appeared on the cell surface; at 4 min, the ligands began to be internalized; and at 30 min, a strong punctuate fluorescence signal appeared inside the cells. These vesicles are contiguous with lysosomes (Fig. S4*C*).

Table 1. K_i and K_d values for binding of htMVL 1 and htMVL 2 (bivalent vs. monovalent)

	MC4R cells		Dual Express			CCK2R cells		Dual Express		
Compound	K_i or K_d nM	n[¶]	K_i or K_d nM	n	Fold increase[‡]	K_i or K_d nM	n	K_i or K_d nM	n	Fold increase[‡]
htMVL 1*	353.6 ± 97.1	4	14.6 ± 1.4	4	24.2[§]	237.5 ± 26.5	4	88.9 ± 9.2	4	2.7[§]
htMVL 2[†]	381.4 ± 15.0	3	16.7 ± 2.0	4	22.9[§]	31.3 ± 1.2	3	16.7 ± 2.0	4	1.9[§]

*htMVL1 is expressed as K_i value. For MC4R receptors, K_i values were calculated with the equation $K_i = IC_{50}/(1+([ligand]/K_d)$, where IC_{50} values from competition binding assays; [ligand] = 10 nM Eu-NDP-α-MSH; K_d = 8.3 nM. For CCK2R receptor, where [ligand] = 1 nM Eu-CCK; K_d = 35 nM.
[†]htMVL 2 is expressed as K_d value from saturation binding assay.
[‡]Ratio of monovalent (MC4R or CCK2R cells) to bivalent binding (dual receptor expressing cells).
[§]$P < 0.05$ (MC4R or CCK2R cells vs. dual receptor expressing cells).
[¶]n refers to the number of independent binding experiments.

Cy5 htMVL 1 Specifically Binds to Target Tumors in Vivo. To investigate whether this targeting strategy can be effective in vivo, target and control cells were implanted bilaterally on the flanks of mice to form xenografts. We i.v. injected 0.5–7.5 nmol htMVL 1 per mouse to establish the optimal dosage. At a dose of 2.5 nmol per mouse, the target tumor retained significant fluorescence, and MC1R control tumors had minimally detectable levels. However, at this dose, the CCK2R tumors still retained significant fluorescence, likely owing to their higher expression levels. From 0.5 h to 10 h after injection of 2.5 nmol htMVL 1, strong fluorescence signals were observed on the target tumors (R flank), but not on the MC1R control tumors (L flank) (Fig. 3*A*). At all time points, surface radiance on the target tumors was significantly higher than on the control tumors. The highest fold enhancement (4.5-fold) occurred at 4 h after injection (Fig. 3*B*). To confirm that the fluorescence signal was related to the two target receptors, blocking agents were preinjected (Fig. 3 *C* and *D*). Injection of NDP-α-MSH, CCK8, or both, respectively, led to a reduction in fluorescence signal by 57%, 75%, and 91% (Fig. 3*D*). Because fluorescent signals from whole-animal imaging are often underestimated because of optical hindrance by soft tissue, we also performed ex vivo imaging of excised tumors and organs at 4 h after injection (Fig. 3 *E* and *F*). Consistent with the in vivo imaging results, the htMVL 1 accumulated highly in the target tumor and kidney, whereas uptake in other organs and control tumor were negligible (Fig. 3*F*).

The expression of target genes was confirmed in the tumor xenografts after fluorescence imaging by IHC. The results

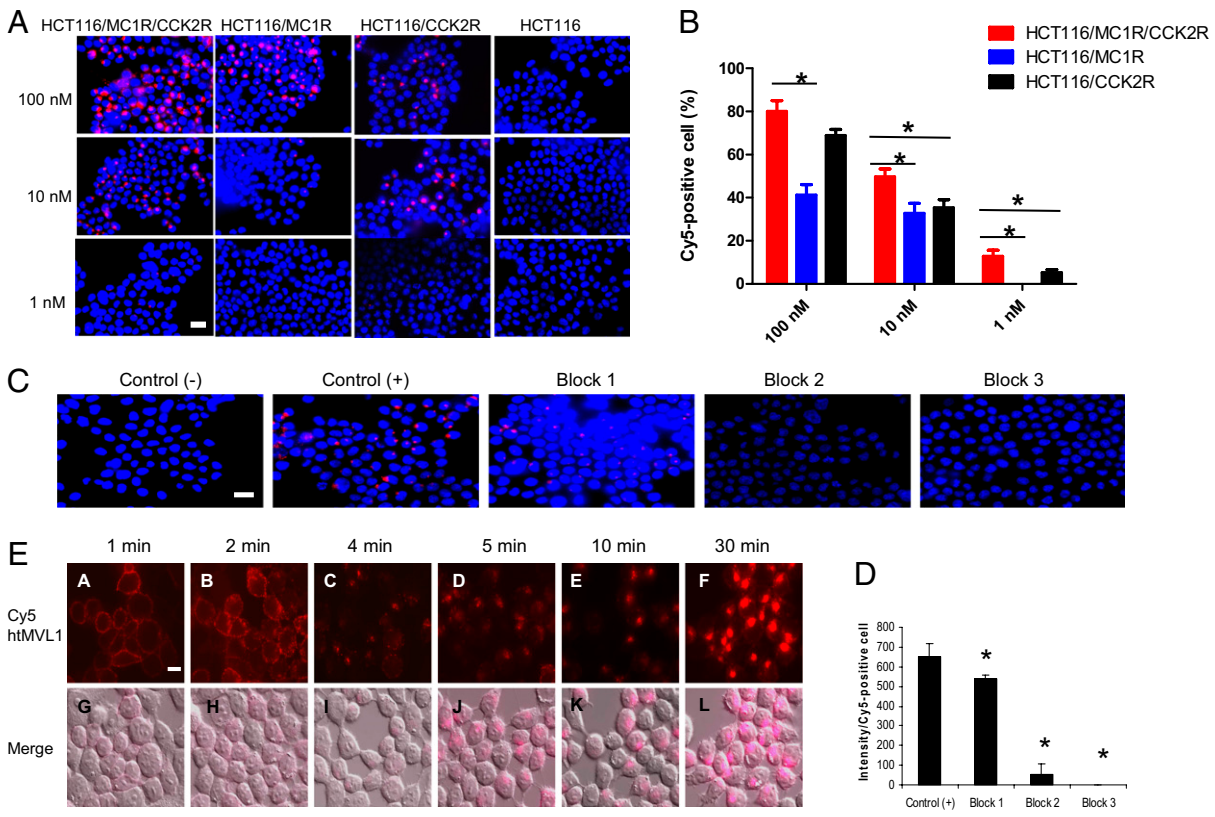

Fig. 2. Live cell imaging of Cy5 htMVL 1 specifically binding to target cells. (*A*) Four types of cells were treated with htMVL 1 at the indicated concentrations for 15 min. Representative live cell fluorescence images of htMVL 1 binding are shown. Red, Cy5; blue, Hoechst. (*B*) The percentage of Cy5-positive cells was determined after htMVL 1 treatments in the target cells (red bars) and control cells (black and blue bars). The data are the mean ± SEM ($n = 3$). A total of ~800 cells were counted for each condition. (*C*) Representative images of blocking study conducted in the target cells. Control (-), no htMVL 1 treatment; Control (+), 10 nM htMVL 1; Block 1: 10 nM htMVL 1 + 10 μM NDP-α-MSH; Block 2: 10 nM htMVL 1 + 10 μM CCK8; Block 3: 10 nM htMVL 1 + 10 μM CCK8 + 10 μM NDP-α-MSH. (*D*) A total of ~600 cells were counted for each condition. The data are shown as mean ± SEM ($n = 3$), *$P < 0.05$. (*E*) htMVL 1 ligand was processed and internalized over time after incubation in the target cells. (*A*–*F*) Cy5 fluorescence images (red). (*G*–*L*) Cy5 fluorescence images merged with a visible light image. (Scale bars: 25 μm.)

showed clear MC1R and CCK2R staining in the corresponding cell lines. Similar CD31 staining was observed in all tumor types, suggesting comparable vascularization for uniform delivery of the ligands (Fig. S4*A*).

Eu htMVL 2 Specifically Binds to Target Tumors. A limitation of the above studies was the inability to quantify the biodistribution or pharmacokinetics at lower doses, which are expected to provide greater discrimination. Additionally, there was concern over the rapid disappearance of the fluorescence signal from the target tumor. Fluorescence was eliminated completely by 24 h after injection, and prior work with a fluorescently labeled delta-opioid targeted antagonist showed retention of signal beyond 120 h (26). We hypothesized that disappearance of the Cy5 htMVL 1 signal in vivo might be due to acid quenching of fluorescence after internalization, as observed in the in vitro Cy5 htMVL 1 related imaging (see above). To investigate this possibility, a Eu-labeled htMVL 2 was used. Although Eu must be measured ex vivo after extraction, its luminescence is not acid quenched and as few as 200 ξmoles Eu can be detected by time-resolved fluorometry (TRF) (27, 28). We injected 2.5 nmol or 0.5 nmol htMVL 2 into tumor-bearing mice, and Eu amounts were measured at 4 h, 24 h, and 48 h after injection from tumors and organs by TRF (29, 30). Standard curves were used to quantitatively relate TRF intensities to Eu levels, which were subsequently normalized to fmol Eu per milligram of tissue (Fig. S4*B* and Tables S2–4). With the same dose of htMVL 2 (2.5 nmol) as the above-described htMVL 1, we observed a higher fold enhancements of 7.4, 3.6, and 4.7-fold at 4 h, 24 h, and 48 h after injection, respectively, compared with 4.5-, 1.8-, and 2.0-fold with htMVL 1 (Figs. 4*A* and 3*B*). However, no enhancement was observed with this dose injection in the mice bearing target tumors versus CCK2R control tumors at the indicated time point (Fig. 4*C*), which was consistent with fluorescence imaging of htMVL 1. Notably, a lower dose (0.5 nmol) resulted in a much higher fold enhancement ratio compared with MC1R control tumors of 12.7-, 6.6-, and 5.2-fold at 4 h, 24 h, and 48 h after injection (Fig. 4*B*). This lower dose also led to higher tumor uptake of htMVL 2 in the target tumors compared with CCK2R control tumors of 5.9-, 6.0-, and 6.2-fold at 4 h, 24 h, and 48 h after injection (Fig. 4*D*). These data are consistent with the hypotheses that disappearance of fluorescence signal was associated with dye quenching or metabolism, and that lower doses of htMVLs provide greater ability to discriminate cells with two, compared with one, cognate receptors.

To determine that the tumor uptake of htMVL 2 was associated to the two target receptors, blocking agents were preinjected before injection of htMVL 2 (Fig. 4*E*). These blocking experiments revealed that Eu uptake was significantly reduced by 65%, 73%, and 78% by injection of NDP-α-MSH, CCK8, and both, respectively, compared with target tumors without any blocking agent treatment (Fig. 4*E*). These data suggest that the uptake with Eu-labeled conjugate was associated with the two target receptors and further confirmed the high selectivity of the heterobivalent ligand targeting in the mouse xenograft model.

Eu uptake in the kidney, and lower but measurable uptake in the liver, were also observed (Fig. 4 *F* and *G*). The amounts of Eu in the kidney were significantly lower at 48 h after injection compared with 4 h and 24 h, which may indicate clearance. Blocking experiments (Fig. 3*C*) had no effect on the signal from kidney, whereas there was a significant decrease of the signal from the target tumor, suggesting that renal uptake was nonspecific.

Mathematical models were applied to calculate whether multivalency can explain increased enhancement at low doses (Fig. S5 and *SI Materials and Methods*) (31). The model results captured the trend of the measured data and also show that multivalency

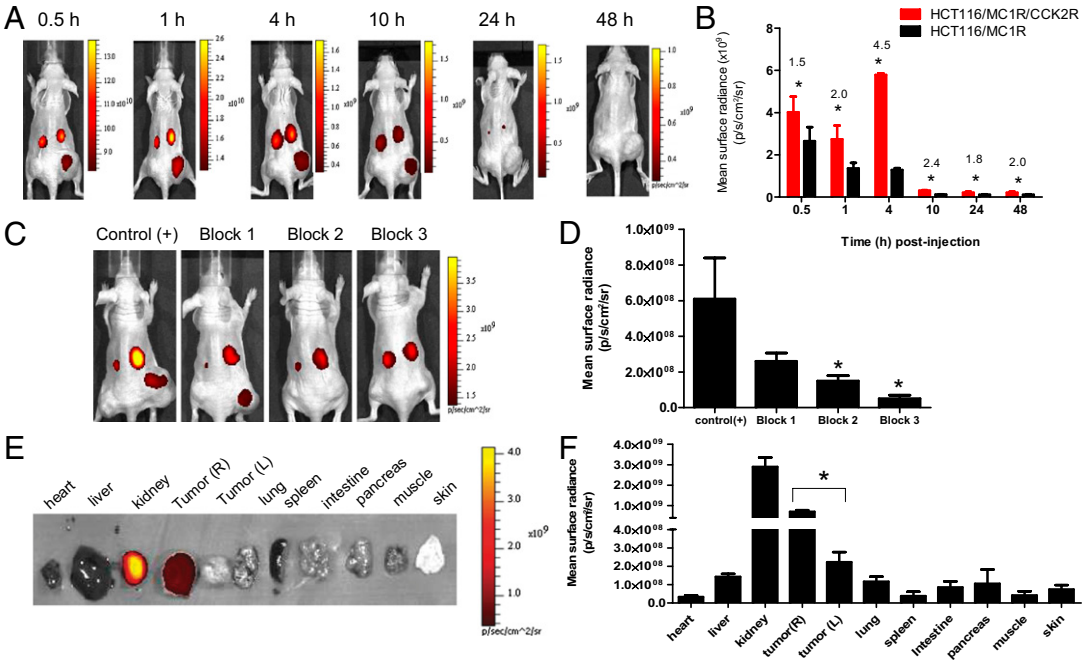

Fig. 3. In vivo fluorescence imaging of Cy5 htMVL 1 specifically retained in target tumors. (*A*) Representative time course of fluorescence images of the Cy5 htMVL 1 retained in mice bearing xenograft tumors. R flank, target tumor; L flank, control tumor (MC1R control). (*B*) Mean surface radiance of htMVL 1 (2.5 nmol per mouse) in the target tumors (red bars) and control tumors (black bars) was quantified at the indicated postinjection time points. Fold increase of mean surface radiance in target relative to control tumors (number shown above asterisks) is shown. Error is expressed as SEM ($n = 4$). (*C*) Representative images of blocking experiments. Control (+) ($n = 4$): 2.5 nmol htMVL 1 per mouse; Block 1 ($n = 3$): 2.5 nmol htMVL 1 + 50 nmol NDP-α-MSH; Block 2 ($n = 5$): 2.5 nmol htMVL 1 + 50 nmol CCK8; Block 3 ($n = 3$): 2.5 nmol htMVL 1 + 50 nmol CCK8 + 50 nmol NDP-α-MSH. (*D*) Mean surface radiance for each target tumor (R flank) under each condition. Error is reported as SEM. Block 2 and block 3 agents lead to significantly decreased signal compared with control tumors (without blocking). (*E*) Representative ex vivo image of tumors and organs excised 4 h after injection of 2.5 nmol htMVL 1. Tumor (R): target tumor; Tumor (L): control tumor. (*F*) Mean surface radiance for each organ. Error is expressed as SEM ($n = 6$), $^*P < 0.05$.

alone could account for the fold enhancement of the 0.5 nmol injection being greater than that of the 2.5 nmol injections.

Discussion

Herein describes a study testing the feasibility of enhanced specificity targeting tumor cells using heterobivalent ligands. Previous work has demonstrated that two functionally unrelated GPCRs, i.e., MC4R and CCK2R, or MC4R and the δ-opioid receptor (δ-OR), can be noncovalently cross-linked by their corresponding heterobivalent ligands with high avidity (12, 17, 19). Multivalency can increase binding avidity, but not necessarily increase targeting specificity (32, 33). By following the previous in vitro findings, the current work studied the parameters including linker length and flexibility, surface receptor expression level per cell, ratio of receptor expression level, receptor-ligand affinity, and ligand concentration on which this targeting specificity depends.

The linker, Pego-$[PG]_3$-Pego, a combination of rigid and flexible linker, demonstrated dynamic mobility over time and temperature ranges and spanned distances of 30~70 Å as predicted by computer models (Fig. 1 *B–D*). As evidenced by the in vitro binding results, this linker structure allowed both side ligands of the heterobivalent compounds, htMVL 1 and htMVL 2, to reach and simultaneously bind to adjacent receptors, resulting in an avidity enhancement of bivalent compared to monovalent binding modes. We have proposed (11, 16) and modeled (15) that maximal specificity of heterobivalent targeting could be achieved with target cells that express both receptor types at similar levels within the range of receptors per cell observed in human cancer (~400–10,000) (34), whereas control cells could express one or the other marker with expression levels comparable to those found in the dual expressing tumors. However, heterogeneity of expression is expected to be common in human tumors, and receptor numbers may not be equivalent or uniform. We were unable to produce cells with equivalent expression levels of the two target receptors. However, such discrepancies are likely to be common in vivo. Thus, although this model system was not optimal, it may reflect the native distribution of target receptors and, thus, enabled us to determine the specificity that could potentially be achieved in patients.

Regardless of expression levels or affinities, optimization of this targeting in patients will require maintaining the ligand levels at doses much lower than the K_d for the highest affinity monomer. In this study, we observed that the higher dose of the heterobivalent ligand (2.5 nmol) exhibited no specificity for the dual receptor expressing tumors relative to the tumor that only expressed CCK2R. This observation is in contrast to the 7.4-fold specificity observed for the dual expressing tumor relative to the tumor expressing MC1R alone. This difference was likely due to differences in receptor expression levels among the tumor lines and differences in binding affinities of the two ligands for their corresponding receptor, i.e., the CCK2R number per cell was much higher than MC1R and the CCK2R pharmacophore had higher affinity compared with that for MC1R. Thus, when the heterobivalent ligand was administered at a high dosage, most MC1R sites were occupied because of heterobivalent interactions, but approximately half of the observed signal originated from monovalent binding to the CCK2R receptor from the remaining probe in circulation. In contrast, at lower doses, most binding appeared to be heterobivalent, the heterobivalent constructs exhibited higher specificity for the dual marker expressing tumors relative to the single marker tumors. These conclusions were supported with a mass balance model (Fig. S5). Hence, although fine-tuning ligand affinities to relative and scalar receptor numbers may be possible in well-characterized in vitro systems, such chemistry will be impractical in vivo because receptor numbers will be nonuniform and difficult to quantify. An ideal system will likely contain two (or more) relatively weak pharmacophores (35). Most important, it will be essential that these ligands are provided at small doses to maximally exploit the multivalent avidity enhancement.

The current in vivo studies consistently showed high nonspecific renal uptake of Cy5- or Eu-labeled ligands (Figs. 3*E* and 4 *F* and *G*). Although this result does not invalidate the current proof-of-principle study, it will be imperative to minimize renal uptake if a therapeutic payload is attached. Notably, improved renal clearance of ligands can be achieved with coinjection of *L*-lysine (36) or glycosylation of the ligand (37). Future use of these small molecule multivalent ligands as targeting agents will require that

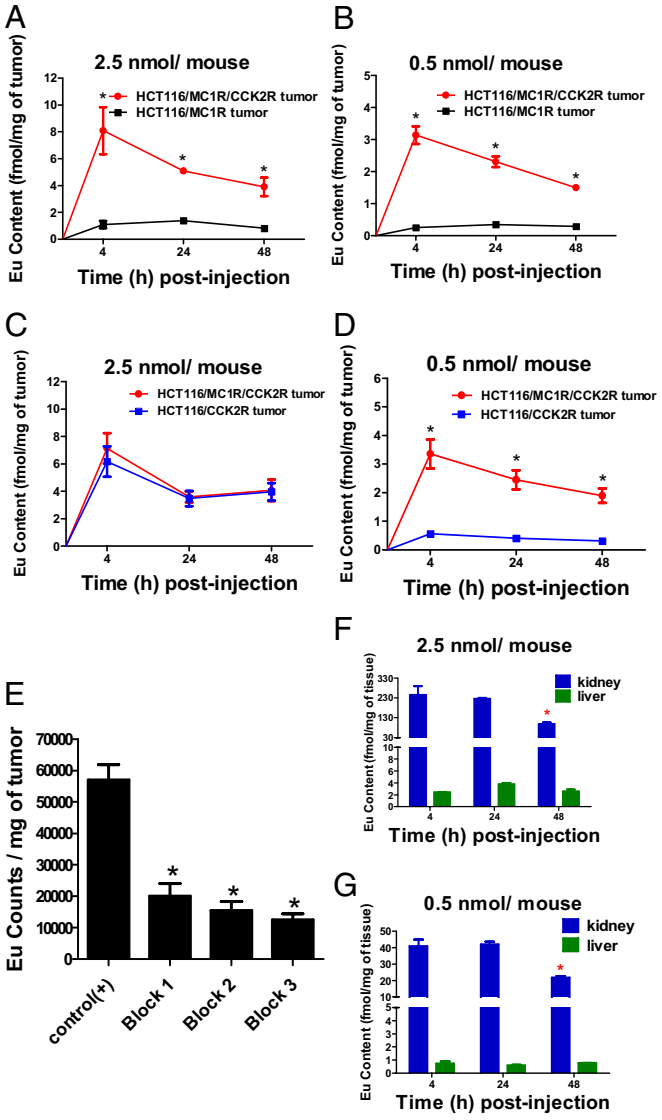

Fig. 4. In vivo quantification of Eu htMVL 2 retained in target tumors. (*A*) Eu content (fmol/mg of tumor) was measured for each tumor from mice injected with 2.5 nmol Eu htMVL 2 as determined by time-resolved fluorometry. The Eu content in target tumors was significantly higher than that in MC1R control tumors. $n = 3$ for each time point. (*B*) Eu content in target tumors versus MC1R control tumors from mice treated with a lower dose (0.5 nmol per mouse). $n = 3$ for each time point. (*C*) Eu content in target tumors versus CCK2R control tumors with 2.5 nmol Eu htMVL 2 treatments. $n = 3$ for each time point. (*D*) Eu content in target tumors versus CCK2R control tumors with 0.5 nmol Eu htMVL 2. $n = 8$ for each time point. (*E*) Eu content was measured in the target tumors under the following conditions: Control (+) ($n = 4$): 0.5 nmol htMVL 2 per mouse; Block 1 ($n = 6$): 0.5 nmol htMVL 2 + 50 nmol NDP-α-MSH; Block 2 ($n = 5$): 0.5 nmol htMVL 2 + 50 nmol CCK8; Block 3 ($n = 5$): 0.5 nmol htMVL 2 + 50 nmol CCK8 + 50 nmol NDP-α-MSH. (*F*) Eu content was measured for the kidney and liver from mice injected with 2.5 nmol of htMVL 2. $n = 3$ for each time point. (*G*) Eu content was also measured with a lower dose (0.5 nmol per mouse) in the kidneys and livers. $n = 3$ for each time point. $^*P < 0.05$.

nonspecific renal uptake be reduced. Further studies will be needed to determine the circulation time of these multivalent constructs in the blood, bioavailability in tissues and organs, potential activation of the immune system, and toxicity. In addition, a better understanding of cell-surface receptor expression levels in patient tumors and normal tissues will need to be developed.

The synthetic heterobivalent ligands developed in this study are relatively small (<5 kDa), highly active binders that display a tumor selectivity due to the multivalent effect. Hence, the primary goal of this study was achieved. This design is a successful application of heteromultivalency to in vivo targeting of two functionally unrelated GPCRs on the cell surface using small synthetic ligands (Fig. S1*A*). The in vitro and in vivo fluorescence imaging with Cy5-conjugated htMVL show a direct visualization of the binding results and a clear demonstration of binding and cross-linking of the complementary receptor combination on target cells with enhanced specificity. This high specificity was further quantified and confirmed by analysis of excised tumors and organs for the presence of the Eu-conjugated htMVL. These findings open the possibility for development of new multivalent agents targeted to unique receptor combinations in tumor cells with a high degree of specificity. Although targeting of tumor cells was the focus of this work, this approach need not be limited to targeting cancers, but may also be useful for targeting other therapies to nonmalignant pathologies.

Materials and Methods

All animal experiments were performed under a protocol approved by the University of South Florida Institutional Animal Care and Use Committee.

HCT116 cells stably expressing MC1R or CCK2R or both were made in our laboratory. The ligands were synthesized by using N^{α}-Fmoc/tBu strategy (17) and molecular dynamic profiling for assessing ligand mobility was performed as described (38–40). Stable HCT116 tumor cell lines were characterized by time-resolved fluorescence (TRF) binding assays and receptor densities determined for each cell line as described (19).

In vivo imaging experiments were performed on female nu/nu mice (Harlan) bearing the target and control tumors by using a Perkin-Elmer IVIS 200 imaging system. The mice received tail vein injection of htMVL 1 and were imaged at various time points after injection. Ex vivo experiments of htMVL 2 were conducted in the same tumor-bearing mice model. Eu was measured from the harvested tumors and tissues using TRF.

Receptor-ligand binding was modeled based on the work by Caplan and Rosca (15, 31). All data were expressed as mean ± SEM. Statistical significance was determined by using two-tailed t test with a significance level of $P < 0.05$.

Further details on experimental and analytical methods (see also Dataset S1) are provided in *SI Materials and Methods*.

ACKNOWLEDGMENTS. We thank J. J. Johnson and M. C. Lloyd at the Moffitt Cancer Center Analytic Microscopy core facility for help with in vitro fluorescence imaging, the University of South Florida Division of Comparative Medicine for help with in vivo imaging related animal work, and the Moffitt Cancer Center Flow Cytometry Core facility for flow cytometry support. The work was supported by National Institutes of Health, National Cancer Institute Grants R01 CA123547 and R01 CA097360 (to R.J.G. and D.L.M.).

1. Strebhardt K, Ullrich A (2008) Paul Ehrlich's magic bullet concept: 100 years of progress. *Nat Rev Cancer* 8(6):473–480.
2. Winau F, Westphal O, Winau R (2004) Paul Ehrlich—in search of the magic bullet. *Microbes Infect* 6(8):786–789.
3. Ferrara N, Hillan KJ, Gerber HP, Novotny W (2004) Discovery and development of bevacizumab, an anti-VEGF antibody for treating cancer. *Nat Rev Drug Discov* 3(5): 391–400.
4. Ginj M, et al. (2005) Preclinical evaluation of new and highly potent analogues of octreotide for predictive imaging and targeted radiotherapy. *Clin Cancer Res* 11(3): 1136–1145.
5. Shadidi M, Sioud M (2003) Selective targeting of cancer cells using synthetic peptides. *Drug Resist Updat* 6(6):363–371.
6. Kiessling LL, Gestwicki JE, Strong LE (2000) Synthetic multivalent ligands in the exploration of cell-surface interactions. *Curr Opin Chem Biol* 4(6):696–703.
7. Mammen M, Choi S, Whitesides G (1998) Polyvalent interactions in biological systems: Implications for design and use of multivalent ligands and inhibitors. *Angew Chem Int Ed* 37(20):2754–2794.
8. Rao J, Lahiri J, Isaacs L, Weis RM, Whitesides GM (1998) A trivalent system from vancomycin.D-ala-D-Ala with higher affinity than avidin.biotin. *Science* 280(5364): 708–711.
9. Hong S, et al. (2007) The binding avidity of a nanoparticle-based multivalent targeted drug delivery platform. *Chem Biol* 14(1):107–115.
10. Thomas TP, et al. (2005) Targeting and inhibition of cell growth by an engineered dendritic nanodevice. *J Med Chem* 48(11):3729–3735.
11. Gillies RJ, Hruby VJ (2003) Expression-driven reverse engineering of targeted imaging and therapeutic agents. *Expert Opin Ther Targets* 7(2):137–139.
12. Vagner J, et al. (2008) Heterobivalent ligands crosslink multiple cell-surface receptors: The human melanocortin-4 and delta-opioid receptors. *Angew Chem Int Ed Engl* 47(9):1685–1688.
13. Bostrom J, et al. (2009) Variants of the antibody herceptin that interact with HER2 and VEGF at the antigen binding site. *Science* 323(5921):1610–1614.
14. Thakur A, Lum LG (2010) Cancer therapy with bispecific antibodies: Clinical experience. *Curr Opin Mol Ther* 12(3):340–349.
15. Caplan MR, Rosca EV (2005) Targeting drugs to combinations of receptors: A modeling analysis of potential specificity. *Ann Biomed Eng* 33(8):1113–1124.
16. Handl HL, et al. (2004) Hitting multiple targets with multimeric ligands. *Expert Opin Ther Targets* 8(6):565–586.
17. Josan JS, et al. (2011) Cell-specific targeting by heterobivalent ligands. *Bioconjug Chem* 22(7):1270–1278.
18. Balagurunathan Y, et al. (2008) Gene expression profiling-based identification of cell-surface targets for developing multimeric ligands in pancreatic cancer. *Mol Cancer Ther* 7(9):3071–3080.
19. Xu L, et al. (2009) Enhanced targeting with heterobivalent ligands. *Mol Cancer Ther* 8(8):2356–2365.
20. Li J, Edwards PC, Burghammer M, Villa C, Schertler GF (2004) Structure of bovine rhodopsin in a trigonal crystal form. *J Mol Biol* 343(5):1409–1438.
21. Palczewski K, et al. (2000) Crystal structure of rhodopsin: A G protein-coupled receptor. *Science* 289(5480):739–745.
22. Abuchowski A, McCoy JR, Palczuk NC, van Es T, Davis FF (1977) Effect of covalent attachment of polyethylene glycol on immunogenicity and circulating life of bovine liver catalase. *J Biol Chem* 252(11):3582–3586.
23. Bentley MD, Bossard MJ, Burton KW, Viegas TX (2008) Poly(ethylene)glycol conjugates of biopharmaceuticals in drug deliver. *Modern Biopharmaceuticals: Design, Development and Optimization*, ed Knablein J (Wiley, Weinheim, Germany), pp 1393–1418.
24. Gabizon A, Shmeeda H, Barenholz Y (2003) Pharmacokinetics of pegylated liposomal Doxorubicin: Review of animal and human studies. *Clin Pharmacokinet* 42(5): 419–436.
25. Smith J (2012) Cellular processing and stability of a CCK/MSH bivalent ligand. Master's thesis (University of Arizona, Tucson).
26. Josan JS, et al. (2009) Solid-phase synthetic strategy and bioevaluation of a labeled delta-opioid receptor ligand Dmt-Tic-Lys for in vivo imaging. *Org Lett* 11(12):2479–2482.
27. Inglese J, et al. (1998) Chemokine receptor-ligand interactions measured using time-resolved fluorescence. *Biochemistry* 37(8):2372–2377.
28. Selvin PR (2002) Principles and biophysical applications of lanthanide-based probes. *Annu Rev Biophys Biomol Struct* 31:275–302.
29. Appel E, Rabinkov A, Neeman M, Kohen F, Mirelman D (2011) Conjugates of daidzein-alliinase as a targeted pro-drug enzyme system against ovarian carcinoma. *J Drug Target* 19(5):326–335.
30. Mignet N, et al. (2006) Liposome biodistribution by time resolved fluorimetry of lipophilic europium complexes. *Eur Biophys J* 35(2):155–161.
31. Shewmake TA, Solis FJ, Gillies RJ, Caplan MR (2008) Effects of linker length and flexibility on multivalent targeting. *Biomacromolecules* 9(11):3057–3064.
32. David A, Kopecková P, Minko T, Rubinstein A, Kopecek J (2004) Design of a multivalent galactoside ligand for selective targeting of HPMA copolymer-doxorubicin conjugates to human colon cancer cells. *Eur J Cancer* 40(1):148–157.
33. Vagner J, Handl HL, Gillies RJ, Hruby VJ (2004) Novel targeting strategy based on multimeric ligands for drug delivery and molecular imaging: Homooligomers of alpha-MSH. *Bioorg Med Chem Lett* 14(1):211–215.
34. Siegrist W, et al. (1989) Characterization of receptors for alpha-melanocyte-stimulating hormone on human melanoma cells. *Cancer Res* 49(22):6352–6358.
35. Brabez N, et al. (2011) Design, synthesis, and biological studies of efficient multivalent melanotropin ligands: Tools toward melanoma diagnosis and treatment. *J Med Chem* 54(20):7375–7384.
36. DePalatis LR, Frazier KA, Cheng RC, Kotite NJ (1995) Lysine reduces renal accumulation of radioactivity associated with injection of the [177Lu]alpha-[2-(4-aminophenyl) ethyl]-1,4,7,10-tetraaza-cyclodecane-1,4,7,10-tetraacetic acid-CC49 Fab radioimmunoconjugate. *Cancer Res* 55(22):5288–5295.
37. Haubner R, et al. (2001) Glycosylated RGD-containing peptides: Tracer for tumor targeting and angiogenesis imaging with improved biokinetics. *J Nucl Med* 42(2): 326–336.
38. Mohamadi F, et al. (1990) Macromodel-an integrated software system for modeling organic and bioorganic molecules using molecular mechanics. *J Comput Chem* 11(4): 440–467.
39. Jonathan M, Goodman W, Still C (1991) An unbounded systematic search of conformational space. *J Comput Chem* 12(9):1110–1117.
40. Guarnieri F, Still WC (1994) A rapid convergent simulation method: Mixed monte carlo/stochastic dynamics. *J Comput Chem* 15(11):1302–1310.